

THE TIP OF THE RED GIANT BRANCH DISTANCES TO TYPE IA SUPERNOVA HOST GALAXIES. V. NGC 3021, NGC 3370, AND NGC 1309 AND THE VALUE OF THE HUBBLE CONSTANT

IN SUNG JANG AND MYUNG GYOON LEE

Astronomy Program, Department of Physics and Astronomy, Seoul National University, Gwanak-gu, Seoul 151-742, Korea

Draft version February 7, 2017

ABSTRACT

We present final results of a program for the determination of the Hubble constant based on the calibration of the Type Ia supernovae (SNe Ia) using the Tip of the Red Giant Branch (TRGB). We report TRGB distances to three SN Ia host galaxies, NGC 3021, NGC 3370, and NGC 1309. We obtain F555W and F814W photometry of resolved stars from the archival *Hubble Space Telescope* data. Luminosity functions of red giant stars in the outer regions of these galaxies show the TRGB to be at $I \approx QT = 28.2 \sim 28.5$ mag. From these TRGB magnitudes and the revised TRGB calibration based on two distance anchors (NGC 4258 and the LMC) in Jang & Lee (2017), we derive the distances: $(m - M)_0 = 32.178 \pm 0.033$ for NGC 3021, 32.253 ± 0.041 for NGC 3370, and 32.471 ± 0.040 for NGC 1309. We update our previous results on the TRGB distances to five SN Ia host galaxies using the revised TRGB calibration. By combining the TRGB distance estimates to SN Ia host galaxies in this study with the SN Ia calibration provided by Riess et al. (2011), we obtain a value of the Hubble constant: $H_0 = 71.66 \pm 1.80(\text{random}) \pm 1.88(\text{systematic}) \text{ km s}^{-1} \text{ Mpc}^{-1}$ (a 3.6% uncertainty including systematics) from all eight SNe, and $H_0 = 73.72 \pm 2.03 \pm 1.94 \text{ km s}^{-1} \text{ Mpc}^{-1}$ (a 3.8% uncertainty) from six low-reddened SNe. We present our best estimate, $H_0 = 71.17 \pm 1.66 \pm 1.87 \text{ km s}^{-1} \text{ Mpc}^{-1}$ (a 3.5% uncertainty) from six low-reddened SNe with the recent SN Ia calibration in Riess et al. (2016). This value is between those from the Cepheid calibrated SNe Ia and those from the Cosmic Microwave Background (CMB) analysis, lowering the Hubble tension.

Subject headings: galaxies: distances and redshifts — galaxies: individual (NGC 3370, NGC 3021 and NGC 1309) — galaxies: stellar content — supernovae: general — supernovae: individual (SN 1994ae, SN 1995al, and SN 2002fk)

1. INTRODUCTION

Measuring the value of the Hubble constant (H_0) is a fundamental step in extragalactic astronomy and cosmology. Tremendous work has been conducted over the past few decades to accurately determine the value of the Hubble constant. However, the estimated values have been controversial until recently. In the 20th century, two groups led by Allan Sandage and Gerard de Vaucouleurs, respectively, measured the value of the Hubble constant to be between $H_0 = 50$ and $100 \text{ km s}^{-1} \text{ Mpc}^{-1}$ (de Vaucouleurs & Peters 1981; de Vaucouleurs 1993; Sandage & Tammann 1974a,b,c,d, 1975a,b, 1976; van den Bergh 1960a,b, 1975, 1994). This was known as "the factor of two controversy". Although it is not clear that this large discrepancy of H_0 originated from a purely scientific result or from a publication bias, the value of H_0 has settled down to a value between the two, $H_0 \sim 70 \text{ km s}^{-1} \text{ Mpc}^{-1}$, with the advent of the *Hubble Space Telescope* (HST).

The Hubble Key Project played a key role in the calibration of H_0 (Freedman et al. 2001). They improved the luminosity calibration of Type Ia Supernovae (SNe Ia) with the HST and yielded a value of $H_0 = 71 \pm 2(\text{random}) \pm 6(\text{systematic}) \text{ km s}^{-1} \text{ Mpc}^{-1}$. A few years later, however, the SN HST project presented a somewhat lower value, $H_0 = 62.3 \pm 1.3(\text{random}) \pm 5.0(\text{systematic}) \text{ km s}^{-1} \text{ Mpc}^{-1}$ (Sandage et al. 2006) from nearly the same HST imaging data as used in the

Hubble Key Project. The level of difference is $\sim 1.5\sigma$. Recent estimations by the Supernovae and H0 for the Equation of State (SH0ES) and the Carnegie Hubble Program provided more precise values: $H_0 = 73.8 \pm 2.4 \text{ km s}^{-1} \text{ Mpc}^{-1}$ (Riess et al. 2011), $H_0 = 73.02 \pm 1.79 \text{ km s}^{-1} \text{ Mpc}^{-1}$ (Riess et al. 2016), and $H_0 = 74.3 \pm 2.1 \text{ km s}^{-1} \text{ Mpc}^{-1}$ (Freedman et al. 2012), respectively. These three estimations that are based on Cepheid calibrated SNe Ia agree remarkably well.

However, the value of H_0 is still considered to be controversial. Recent analysis of the cosmic microwave background radiation (CMBR) with a flat Λ CDM cosmology by WMAP and PLANCK groups yielded values of H_0 with remarkably small uncertainties: $H_0 = 69.3 \pm 0.8 \text{ km s}^{-1} \text{ Mpc}^{-1}$ from WMAP9 (Bennett et al. 2013) and $H_0 = 67.8 \pm 0.9 \text{ km s}^{-1} \text{ Mpc}^{-1}$ from PLANCK (Planck Collaboration et al. 2015), which are lower than the values based on Cepheid calibrated SNe. Moreover, recent studies of the baryon acoustic oscillation (BAO) combined with SNe Ia data yielded a value similar to those from the CMBR analysis, $H_0 = 67.3 \pm 1.1 \text{ km s}^{-1} \text{ Mpc}^{-1}$ (Aubourg et al. 2015). These three estimations agree well. However, these values are $2 \sim 3\sigma$ smaller than those from Cepheid calibrated SNe Ia. Note that CMBR and BAO are inverse distance ladders, while Cepheids and SN Ia are classical distance ladders. This discrepancy between the results based on the inverse distance ladder method and the classical distance ladder method is now one of the critical issues in modern cosmology. It is needed to check systematics of both the classical and

TABLE 1
A SUMMARY OF *HST* OBSERVATIONS OF SNE IA CALIBRATION SAMPLE

Target	R.A. (J2000.0)	Decl. (J2000.0)	Instrument	Exposure time		Prop. ID
				F555W	F814W	
NGC 3021	09 51 00.71	33 33 23.9	ACS/WFC	61,760s	24,000s	10497
NGC 3370	10 47 06.91	17 16 40.0	ACS/WFC	61,240s	24,000s	9651
NGC 1309	03 22 05.31	-15 23 47.8	ACS/WFC	61,760s	24,000s	10497

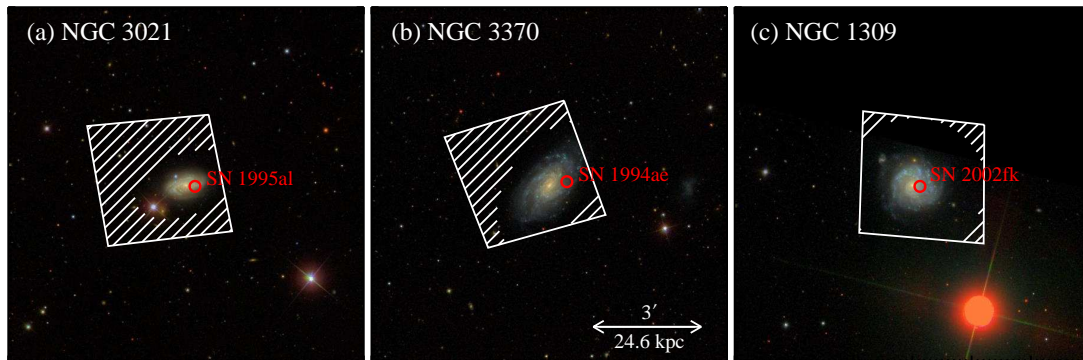


FIG. 1.— Identification of HST/ACS fields of NGC 3021, NGC 3370, and NGC 1309 used in this study overlaid on the $10' \times 10'$ color maps provided by the Sloan Digital Sky Survey. Locations of the SNe Ia are marked by open circles. Hatched regions in each HST field represent the halo regions used for the TRGB analysis.

inverse distance ladder methods in order to understand what may cause this discrepancy.

We have been working to improve the measurement of H_0 by measuring the accurate luminosity of SN Ia based on the Tip of the Red Giant Branch (TRGB), as part of the program, the TRGB distances to SN host galaxies in the Universe (TIPSNU). The TRGB is known as a precise population II distance indicator (Lee et al. 1993; Freedman & Madore 2010; Jang & Lee 2017; Beaton et al. 2016). Lee & Jang (2012, 2013) (Papers I and II) determined the TRGB distances to three SNe Ia host galaxies: M101, M66, and M96 hosting SN 2011fe, SN 1989B, and SN 1998bu, respectively. In Paper III, Jang & Lee (2015) derived the TRGB distances to two additional SN Ia host galaxies: NGC 4038/39 and NGC 5584 hosting SN 2007sr and SN 2007af, respectively. By combining the TRGB distances to five SN Ia host galaxies with optical light curves for five SNe Ia in these galaxies, we obtained a value of the Hubble constant, $H_0 = 69.8 \pm 2.6(\text{random}) \pm 3.9(\text{systematic}) \text{ km s}^{-1} \text{ Mpc}^{-1}$. In Paper VI, Jang & Lee (2017) presented a revised calibration of the TRGB with a systematic uncertainty of 0.046 mag, much smaller than those of the previous calibrations (~ 0.12 mag). This calibration used, as a distance anchor, NGC 4248 and the LMC to which geometric distances are known with high precision (Humphreys et al. 2013; Riess et al. 2016; Pietrzyński et al. 2013).

In this paper, we present the TRGB distances to three additional galaxies hosting three SNe Ia: NGC 3021 (SA(rs)bc:) hosting SN 1995al, NGC 3370 (SA(s)c) hosting SN 1994ae, and NGC 1309 (SA(s)bc:) hosting SN 2002fk. Spectroscopic observations confirmed that three SNe are normal SNe Ia (Riess et al. 2009a). Light curves of these SNe Ia were obtained with modern CCD detectors, covering their maximum luminosity

epochs. Moreover, the internal extinctions for these SNe are estimated to be small ($A_V \lesssim 0.5$ mag) (Riess et al. 2009a). Thus, these three SNe Ia are excellent targets for the luminosity calibration of SN Ia. Riess et al. (2005, 2009b) carried out deep HST observations for these galaxies to derive Cepheid distances to these galaxies. By combining optical light curves of Cepheid variables with their F160W band luminosities, they determined distances of $(m - M)_0 = 32.498 \pm 0.091$ for NGC 3021, $(m - M)_0 = 32.071 \pm 0.050$ for NGC 3370, and $(m - M)_0 = 32.524 \pm 0.056$ for NGC 1309 (Riess et al. 2016). However, there are no published studies for the TRGB distances to these galaxies.

The outline of this paper is as follows. In Section 2 we describe the data and the data reduction method. Section 3 presents the color-magnitude diagrams (CMDs) and luminosity functions of the resolved stars in three galaxies. These will be used to estimate the TRGB distances. In §4 we present updated TRGB distances to five SN Ia host galaxies included in our previous studies and compare our results with those from the SH0ES project (Riess et al. 2011, 2016). We also derive the absolute magnitude of SNe and the value of the Hubble constant. Primary results are summarized in the final section.

2. DATA AND DATA REDUCTION

Table 1 lists basic information of archival HST images of the three SN Ia host galaxies we used for the TRGB analysis. These galaxies were observed using the same instrument, the Advanced Camera for Surveys (ACS), with a primary aim to detect Cepheid variables (PID=9651, 10497). These ACS fields cover halos as well as bulges and disks of the target galaxies, as shown in **Figure 1**. We constructed master drizzled images of each field from individual images as described in Jang & Lee (2015). We set `final_pixfrac=0.7` and `final_scale=0''.03/pixel` in

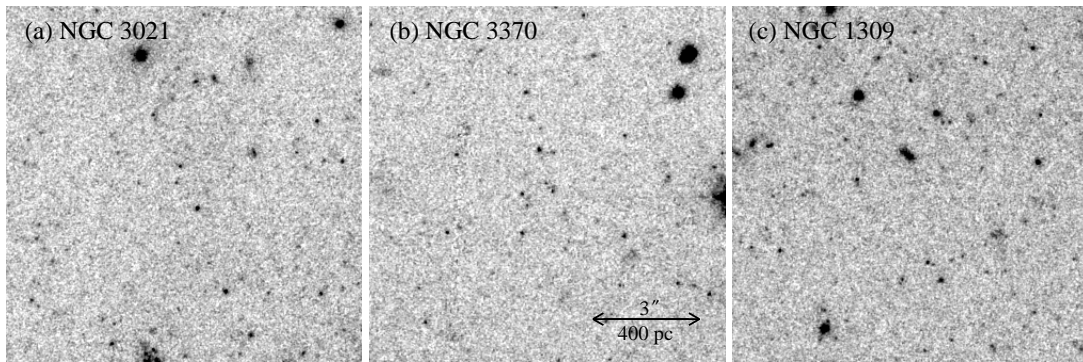


FIG. 2.— $10'' \times 10''$ thumbnails of $F814W$ band drizzled images showing the halo regions of NGC 3021 (a), NGC 3370 (b), and NGC 1309 (c). Note that most of the resolved point sources are old red giants in each galaxy.

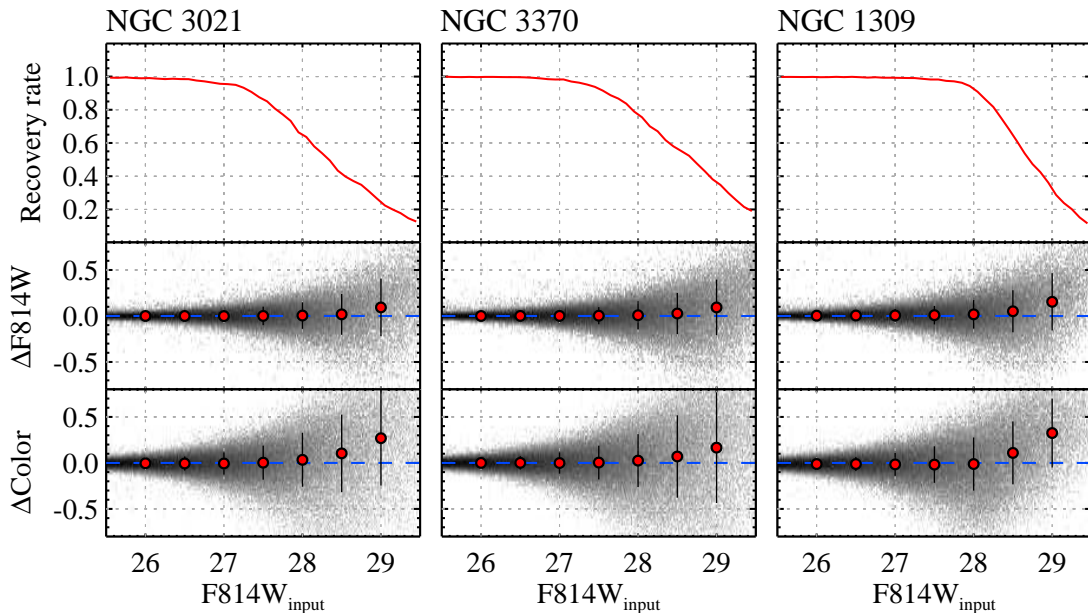


FIG. 3.— (Top panels) Recovery rates for RGB candidates ($F555W - F814W = 1.8$) in NGC 3021 (left), NGC 3370 (middle) and NGC 1309 (right). (Middle and bottom panels) Differences in $F814W$ and $F555W - F814W$ (inputs minus outputs) as a function of input $F814W$ magnitudes. Median offsets and standard deviations in each magnitude bin are marked by circles with vertical lines.

the drizzling, to secure better angular resolution than those of drizzled images from the default setting (`final_pixfrac=1.0` and `final_scale=0.05/pixel`). Total exposure times of each field are $\sim 61,500$ s for $F555W$ band and $24,000$ s for $F814W$ band. **Figure 2** shows $10'' \times 10''$ sections of combined $F814W$ band images we made for an outer region in each galaxy. Resolved stars are clearly seen in each field, and most of the faint resolved stars are old red giant stars in the target galaxies.

Instrumental magnitudes were derived from the standard sequence, `FIND-PHOT-ALLSTAR-ALLFRAME` in the DAOPHOT package (Stetson 1987). PSF images were constructed using $30 \sim 60$ bright isolated stars in the images. Standard calibration of instrumental magnitudes on the HST Vega magnitude system was done using the information provided by the STScI. Detailed reduction methods can be found in our previous papers (Jang & Lee 2015, 2017).

We carried out artificial star experiments to check the completeness and the systematic bias of our photometry. We added artificial stars to the selected regions of HST images that are indicated by hatched regions in **Figure**

1 using the DAOPHOT/ADDSTAR task. The number of added artificial stars are ~ 2000 for NGC 3021 and NGC 3370, and ~ 400 for NGC 1309. These numbers are less than 10% of the total number of stars detected in the same regions. We set $F555W - F814W = 1.8$ for the input artificial stars to make them similar to the mean color of the blue (metal poor) TRGB stars. We then performed photometry as done for real stars and derived recovery rates and photometric offsets. We iterated this process 100 times for NGC 3021 and NGC 3370, and 500 times for NGC 1309 to reduce statistical uncertainties. The total number of artificial stars used for the experiments is $\sim 200,000$ for each galaxy.

Figure 3 displays the result of artificial star experiments for the three galaxies. The 50% recovery rates are estimated to be $F814W \approx 28.35$, 28.70 , and 28.71 mag for NGC 3021, NGC 3370, and NGC 1309, respectively. At the TRGB magnitudes expected from the Cepheid distance estimates in the previous studies (Riess et al. 2011, 2016) ($F814W_{TRGB} = 28.1 \sim 28.5$ mag), the recovery rates are ranging from $\sim 50\%$ (NGC 3021) to $\sim 70\%$ (NGC 3370), somewhat higher

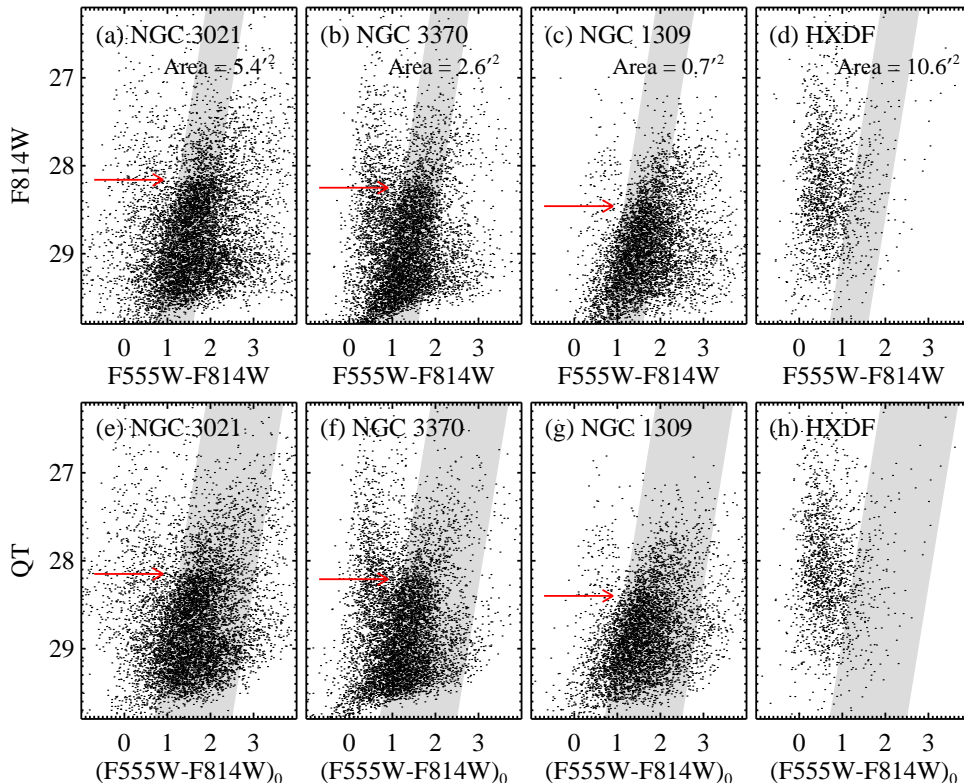


FIG. 4.— (a)-(c) $F814W - (F555W - F814W)$ CMDs of the resolved stars in the halo regions of NGC 3021 (a), NGC 3370 (b), and NGC 1309 (c). We also display a CMD of the point sources in the Hubble eXtreme Deep Field (HXDF) in (d) as a reference. (e)-(h) Same as (a)-(d), except for the QT magnitude with the extinction corrected color, $(F555W - F814W)_0$. The shaded region in each panel denotes the boundary to select the RGB stars for the TRGB analysis. Estimated TRGB magnitudes are marked by red arrows.

than 50%. We detect small magnitude and color offsets. At the expected TRGB level, the $F814W$ magnitudes and $F555W - F814W$ color offsets are measured to be $\Delta F814W_{TRGB} \sim 0.02$ mag and $\Delta(F555W - F814W)_{TRGB} \sim 0.05$ mag for both NGC 3021 and NGC 3370 reductions. The offsets are slightly larger in the case of NGC 1309 reduction: $\Delta F814W_{TRGB} \sim 0.05$ mag and $\Delta(F555W - F814W)_{TRGB} \sim 0.10$ mag. Thus, measured TRGB magnitudes and colors are expected to be slightly brighter and bluer than their intrinsic values. We considered these photometric offsets in the TRGB distance estimation (Section 3.2).

3. RESULTS

3.1. CMDs of Resolved Stars

The HST fields for the target galaxies cover not only the disk but also the halo of each galaxy. In order to sample as many old RGB stars, we selected resolved stars in the outer regions of the target galaxies, as shown by the hatched regions in **Figure 1**. **Figure 4(a-c)** show $F814W - (F555W - F814W)$ CMDs of the resolved stars in the outer regions of NGC 3021 (a), NGC 3370 (b), and NGC 1309 (c). All three CMDs show a prominent RGB population.

It is expected that some of the point sources detected in the images of the target galaxies are unresolved background galaxies. To estimate the background galaxy contamination in the CMDs, we investigated the CMD of the Hubble eXtreme Deep Field (HXDF), which is dominated by distant galaxies, as shown in Lee & Jang (2016). We used combined $F606W$ and $F814W$ images for the

HXDF provided by the XDF project (Illingworth et al. 2013). Then we carried out PSF photometry using the same procedure as done for the target galaxies. We applied the color transformation from $F606W - F814W$ to $F555W - F814W$ using the transformation described in Jang & Lee (2017), to be consistent with the CMDs of the target galaxies.

Figure 4(d) represents the CMD of the point sources in the HXDF. This CMD shows a significant vertical structure in the blue side of the shaded region (the RGB of the target galaxies), while only a small number of sources are seen in the shaded region. This vertical structure represents mainly blue faint background galaxies. The area of the HXDF is 10.6 arcmin^2 , much larger than those of the selected regions for the target galaxies (5.4 arcmin^2 , 2.6 arcmin^2 , and 0.7 arcmin^2 for NGC 3021, NGC 3370, and NGC 1309, respectively). We counted the numbers of bright point sources with $F814W \leq 29$ mag located in the shaded regions, which were chosen to select the RGB population, obtaining 2396, 1991, 1914, and 190 sources for NGC 3021, NGC 3370, NGC 1309, and the HXDF, respectively. Considering the field area ratios, we estimated the fractions of the background galaxies for the target galaxies: 4.0% for NGC 3021, 2.3% for NGC 3370, and 0.6% for NGC 1309. Thus, background galaxy contamination in the shaded regions of the target galaxies is negligible. We ignored the background galaxy contamination in the following TRGB analysis.

Jang & Lee (2017) introduced the QT magnitude, a color (metallicity) corrected RGB magnitude, for a more accurate TRGB calibration. The QT magnitude

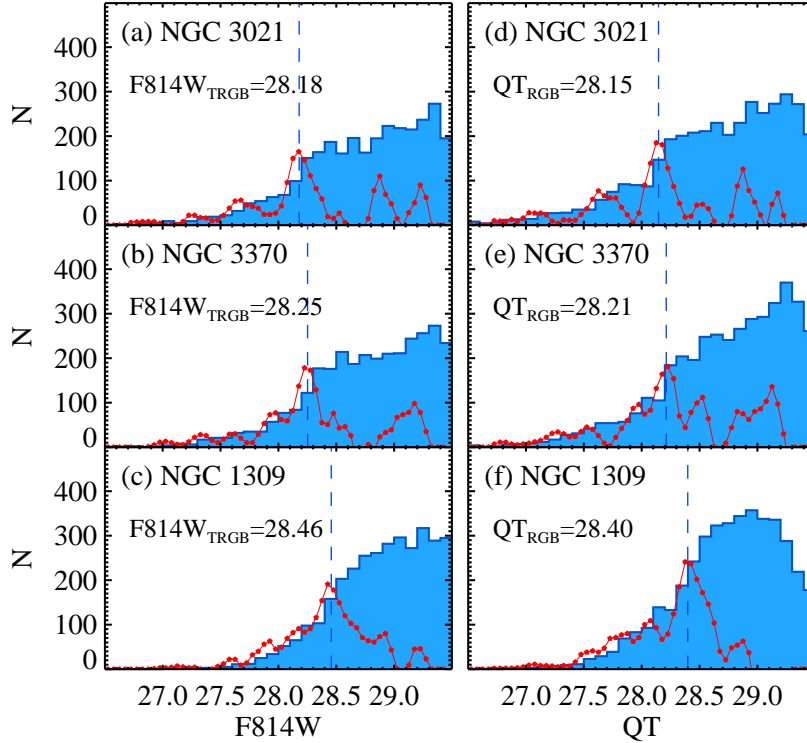


FIG. 5.— (a)-(c) LFs (histograms) and edge detection responses (curved lines) of the RGB stars in NGC 3021 (a), NGC 3370 (b), and NGC 1309 (c). Estimated TRGB magnitudes are marked by vertical dashed lines in each panel. (d)-(f) Same as (a)-(c), except for the QT magnitude.

is defined as $QT = F814W_0 - 0.116(Color - 1.6)^2 + 0.043(Color - 1.6)$, where $Color = (F555W - F814W)_0$ for the ACS/WFC. We plotted QT magnitude versus $(F555W - F814W)_0$ diagrams of the resolved point sources in **Figure 4(e-h)**. Foreground reddenings are known to be very small: $E(B - V) = 0.012, 0.028, 0.035$, and 0.007 for NGC 3021, NGC 3370, NGC 1309, and the HXDF, respectively (Schlafly & Finkbeiner 2011, NASA/IPAC Extragalactic Database). Internal reddenings of the selected outer regions are expected to be negligible so that these are assumed to be zero in this study.

3.2. Distance Estimation

We determined the distances to the target galaxies using the TRGB method (Lee et al. 1993; Madore & Freedman 1995). We selected resolved stars in the shaded regions of **Figure 4**. The shaded regions for $F814W - (F555W - F814W)$ CMDs were designed to sample blue RGB stars with $1.2 \leq F555W - F814W \leq 2.1$ near the TRGB level because the color (metallicity) dependence of the TRGB at the blue side is estimated to be small (Jang & Lee 2017). In the cases of $QT - (F555W - F814W)_0$ CMDs, we set slightly wider shaded regions, sampling RGB stars with $1.2 \leq F555W - F814W \leq 3.0$ near the TRGB level.

Figure 5 displays $F814W$ (a, b, and c) and QT (d, e, and f) luminosity functions of the selected RGB stars in the CMDs. The luminosity functions for all three galaxies show abrupt increments at $F814W \simeq QT = 28.2 \sim 28.5$ mag, which correspond to the TRGB. We applied an edge detection algorithm for the quantitative TRGB detection. We used a Sobel filter employing the zero-sum

kernel of $[-1, -2, -1, 0, +1, +2, +1]$ with a bin size of 0.05 mag. Output edge detection responses are shown as red lines in **Figure 5**.

Mean TRGB magnitudes and associated uncertainties were measured by running 10,000 simulations of bootstrap resampling as done for our previous studies (Lee & Jang 2012, 2013; Jang & Lee 2015). In each simulation, we made a new sample of RGB stars by sampling a half size of stars randomly from the original RGB sample. We obtained TRGB magnitudes from the new samples as done for the original sample. We generated a histogram of the TRGB magnitudes obtained from the simulations and fitted a Gaussian function to the histogram, quoting the gaussian mean as a mean TRGB magnitude and the gaussian width as 1σ uncertainty. Measured TRGB values are: $F814W_{TRGB} = 28.179 \pm 0.049, 28.252 \pm 0.035$ and 28.457 ± 0.044 mag for NGC 3021, NGC 3370, and NGC 1309, respectively. Similarly, $QT_{TRGB} = 28.146 \pm 0.033$ mag for NGC 3021, 28.212 ± 0.041 mag for NGC 3370, and 28.398 ± 0.040 mag for NGC 1309 were obtained. Derived TRGB magnitudes from the QT luminosity functions are systematically brighter than those from $F814W$ luminosity functions, because the QT system uses foreground extinction corrected $F814W$ magnitude ($F814W_0$).

We detected small photometric offsets from the artificial star experiments as described in Section 2. The $F814W$ and the QT magnitude offsets at the TRGB levels of three galaxies are measured to be $\Delta F814W_{TRGB} (\Delta QT_{TRGB}) = 0.010$ (0.021) mag for NGC 3021, 0.018 (0.030) mag for NGC 3370, and 0.048 (0.062) mag for NGC 1309. We corrected these magnitude offsets in the distance estimation. The $F555W - F814W$ color off-

TABLE 2
A SUMMARY OF THE TRGB DISTANCE ESTIMATES TO SN IA HOST GALAXIES

Target	Region	TRGB Magnitude		Offset ^a	$(m - M)_0^b$	$(m - M)_0^b$	$(m - M)_0^b$
		F814W	QT		NGC 4258 scale	LMC scale	NGC 4258 + LMC
Blue I calibration							
M101	Entire field	25.162 ± 0.035	...	0.003	29.185 ± 0.035	29.119 ± 0.035	29.145 ± 0.035
M66	$R_{GC} \geq 4'3^c$	26.232 ± 0.087	...	0.002	30.212 ± 0.087	30.146 ± 0.087	30.175 ± 0.087
M96	$R_{GC} \geq 3'5^c$	26.247 ± 0.064	...	-0.002	30.237 ± 0.064	30.171 ± 0.064	30.189 ± 0.064
NGC 4038/39	Lowest sky ^d	27.696 ± 0.049	...	-0.002	31.663 ± 0.049	31.597 ± 0.049	31.660 ± 0.049
NGC 5584	Lowest sky ^d	27.826 ± 0.060	...	-0.002	31.803 ± 0.060	31.737 ± 0.060	31.784 ± 0.060
NGC 3021	$SMA \geq 1'5$	28.179 ± 0.049	...	0.010	32.198 ± 0.049	32.132 ± 0.049	32.148 ± 0.049
NGC 3370	$SMA \geq 2'0$	28.252 ± 0.035	...	0.018	32.253 ± 0.035	32.187 ± 0.035	32.243 ± 0.035
NGC 1309	$SMA \geq 2'0$	28.457 ± 0.044	...	0.048	32.474 ± 0.044	32.408 ± 0.044	32.469 ± 0.044
QT calibration							
M101	Entire field	...	25.142 ± 0.022	0.003	29.166 ± 0.022	29.147 ± 0.022	29.160 ± 0.022
M66	$R_{GC} \geq 4'3^c$...	26.144 ± 0.038	0.025	30.186 ± 0.038	30.167 ± 0.038	30.180 ± 0.038
M96	$R_{GC} \geq 3'5^c$...	26.199 ± 0.054	0.013	30.229 ± 0.054	30.210 ± 0.054	30.223 ± 0.054
NGC 4038/39	Lowest sky ^d	...	27.647 ± 0.037	0.015	31.683 ± 0.037	31.664 ± 0.037	31.677 ± 0.037
NGC 5584	Lowest sky ^d	...	27.725 ± 0.049	0.006	31.757 ± 0.049	31.738 ± 0.049	31.751 ± 0.049
NGC 3021	$SMA \geq 1'5$...	28.146 ± 0.033	0.021	32.184 ± 0.033	32.165 ± 0.033	32.178 ± 0.033
NGC 3370	$SMA \geq 2'0$...	28.212 ± 0.041	0.030	32.259 ± 0.041	32.239 ± 0.041	32.253 ± 0.041
NGC 1309	$SMA \geq 2'0$...	28.398 ± 0.040	0.062	32.477 ± 0.040	32.457 ± 0.040	32.471 ± 0.040

^a Denotes F814W and the QT magnitude offsets measured from the artificial star experiments.

^b Quoted errors are random errors only. Systematic errors are estimated to be about 0.068 mag for the NGC 4258 scale, 0.104 mag for the LMC scale, and 0.057 mag for both NGC 4258 and the LMC scales (Jang & Lee 2017).

^c Indicates hatched regions shown in Figure 1 of Lee & Jang (2013).

^d Indicates hatched regions shown in Figure 1 of Jang & Lee (2015).

sets we measured at the TRGB levels are ranging from $\Delta(F555W - F814W) = 0.048$ mag (NGC 3370) to 0.104 mag (NGC 1309). We assume that these small color offsets will not significantly effect the TRGB measurements. For example, a color offset of ± 0.1 mag at the mean TRGB color ($= F555W - F814W \sim 1.8$) changes the QT magnitude only by ± 0.003 mag. Thus we ignored the color offsets in the following analysis.

Distance moduli to target galaxies were derived by applying the recent TRGB calibration presented in our previous study, Paper IV (Jang & Lee 2017). Two TRGB calibrations are available: the blue I calibration and the QT calibration. We first apply the blue I calibration, which uses the traditional I (F814W) magnitude for blue RGB stars with $F555W - F814W \leq 2.1$, where the color-dependence of the TRGB is not significant. There are three absolute TRGB zero-points based on the combination of two distance anchors, NGC 4258 and the LMC, to which precise geometric distances are known (Humphreys et al. 2013; Riess et al. 2016; Pietrzyński et al. 2013). Under the photometric system used in this study, the F555W and F814W band combination of ACS/WFC, absolute magnitudes of the TRGB are $M_{F814W,TRGB} = -4.030 \pm 0.068$ mag for the NGC 4258 scale, and $M_{F814W,TRGB} = -3.964 \pm 0.106$ mag for the LMC scale. A weighted mean of these two is $M_{F814W,TRGB} = -4.008 \pm 0.057$ mag. If we adopt this value, we obtain distance moduli of $(m - M)_0 = 32.144 \pm 0.049$ for NGC 3021, $(m - M)_0 = 32.243 \pm 0.035$ for NGC 3370, and $(m - M)_0 = 32.469 \pm 0.044$ for NGC 1309. Systematic uncertainties are estimated to be 0.057 mag.

We also apply the QT calibration that uses the QT magnitude with a wider color range of RGB stars so that more RGB stars can be used for the TRGB analysis. The zero-points for the QT calibration are

$M_{QT,TRGB} = -4.017 \pm 0.067$ mag for the NGC 4258 scale, $M_{QT,TRGB} = -3.998 \pm 0.101$ mag for the LMC scale, and $M_{QT,TRGB} = -4.011 \pm 0.056$ mag for both NGC 4258 and the LMC scales. Adopting the most accurate calibration based on both distance anchors, we obtain $(m - M)_0 = 32.178 \pm 0.033$ for NGC 3021, $(m - M)_0 = 32.253 \pm 0.041$ for NGC 3370, and $(m - M)_0 = 32.471 \pm 0.040$ for NGC 1309. Systematic uncertainties are estimated to be 0.056 mag. **Table 2** lists a summary of distance estimates based on the revised TRGB calibration for the target galaxies in this study. We also included five other galaxies that were covered in our previous studies (Lee & Jang 2012, 2013; Jang & Lee 2015).

4. DISCUSSION

4.1. Updating the TRGB Distances in Our Previous Studies

In Papers I (Lee & Jang 2012), II (Lee & Jang 2013), and III (Jang & Lee 2015), we presented the TRGB distances to five SN Ia host galaxies: M101 (Paper I), M66 and M96 (Paper II), and NGC 4038/39 and NGC 5584 (Paper III). These results were based on the old TRGB calibration (Rizzi et al. 2007). We update these results using the revised TRGB calibration introduced in Paper IV. We carried out PSF photometry on drizzled images (indicated by `_drc.fits`) of the five galaxies using DAOPHOT/ALLFRAME (Stetson 1987, 1994). We used the same HST data set as analyzed in our previous studies, except for M101. In the case of M101, we used new HST/ACS data of a halo field (centered at $(\alpha, \delta) = (14^h 03^m 47.21^s, 54^\circ 14' 25''.6)$) released recently (PID=13364). Exposure times are 1100s for F606W and 1400s for F814W, longer than those used in Paper I ($F555W = 720s \sim 1080s$ and $F814W = 720s \sim 1080s$).

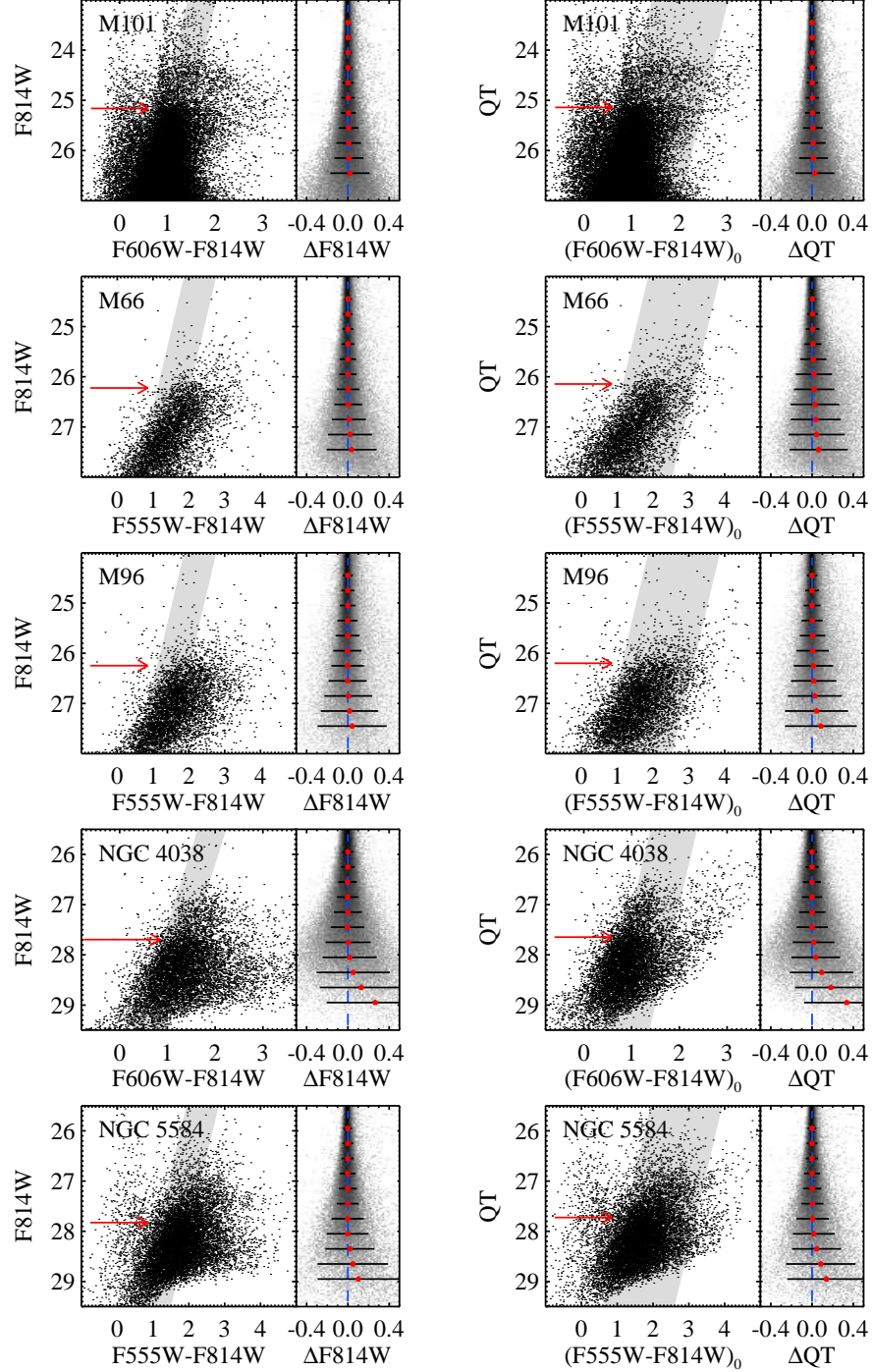


FIG. 6.— Left windows in each panel: $F814W$ (left panels) and the QT (right panels) CMDs of resolved stars in five SN Ia host galaxies used in our previous studies (Lee & Jang 2012, 2013; Jang & Lee 2015). The shaded region in each panel represents the selection criteria for RGB stars. Estimated TRGB magnitudes are marked by red arrows. Right windows in each panel: results of artificial star experiments in $F814W$ (left panels) and in the QT magnitudes (right panels). Mean offsets with standard deviations in each magnitude bin are marked by red dots with horizontal lines.

Figure 6 displays the CMDs with $F814W$ and the QT magnitudes of the resolved stars in the outer regions of M101, M66, M96, NGC 4038/39 and NGC 5584. All of the CMDs show dominant RGB populations, as well as asymptotic giant branch and young main-sequence populations. We carried out artificial star experiments to these five galaxies as done for the three galaxies in Section 2, plotting the results in the right side of each CMD.

We confirmed that the $F814W$ and the QT magnitude offsets at the expected TRGB level are as small as 0.02 mag. We corrected these offsets in the TRGB distance estimation.

We selected the stars in the shaded regions of CMDs in **Figure 6**, producing a sample of RGB stars in each galaxy. Then we plotted their luminosity functions and corresponding edge detection responses in **Figure 7**.

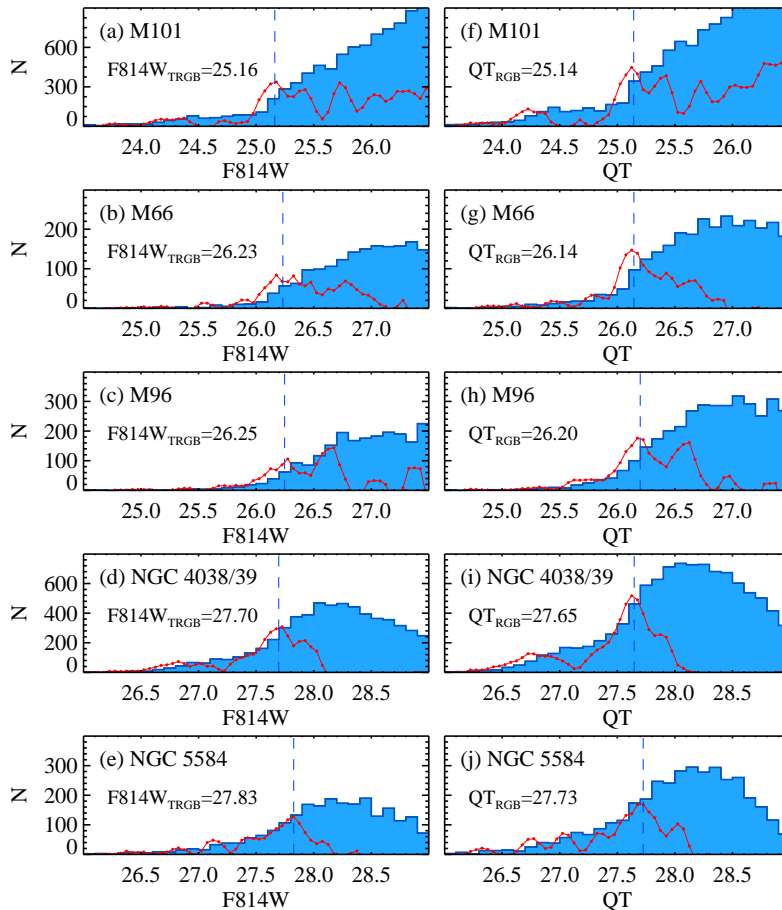


FIG. 7.— (a)-(e) F814W magnitude luminosity functions of RGB stars in the selected regions of five SN Ia host galaxies. Edge detection responses and estimated TRGB magnitudes are indicated by red solid and blue dashed lines, respectively. (f)-(j) Same as (a)-(e) but for the QT magnitude.

The luminosity functions of these galaxies show sudden jumps at $F814W \sim QT \sim 25.2$ (M101), 26.2 (M66 and M96), 27.7 (NGC 4038/39), and 27.8 (NGC 5584), corresponding to the TRGBs. It is noted that the edge detection responses for the QT luminosity functions show stronger and more narrow peaks at the TRGB than those for the $F814W$ luminosity functions. Mean TRGB magnitudes and corresponding errors were measured using the bootstrap resampling method as applied to the three galaxies described in Section 3.2. Derived values of the TRGB magnitudes are: $F814W_{TRGB} = 25.162 \pm 0.035$ for M101, 26.232 ± 0.087 for M66, 26.247 ± 0.064 for M96, 27.696 ± 0.049 for NGC 4038/39, and 27.826 ± 0.060 for NGC 5584. Similarly, we obtain the TRGB magnitudes from the QT luminosity functions: $QT_{TRGB} = 25.142 \pm 0.022$ for M101, 26.144 ± 0.038 for M66, 26.199 ± 0.054 for M96, 27.647 ± 0.037 for NGC 4038/39, and 27.725 ± 0.049 for NGC 5584. Here all errors are random errors. The errors from the QT luminosity functions are, on average, 32% smaller than those of the $F814W$ luminosity functions.

The values of the TRGB magnitudes in the $F814W$ band of these galaxies show excellent agreement ($\Delta(m - M)_0 \lesssim 0.05$) with those in our previous papers, except for M101. In the case of M101, the new estimate of the TRGB magnitude, $F814W_{TRGB} = 25.162 \pm 0.035$, is, 0.118 mag brighter than the value in Lee & Jang (2012),

$I_{TRGB} = 25.28 \pm 0.01$. Main causes for this difference can be explained as follows. First is the difference in the values of the aperture correction for photometry. We adopted a value of 0.098 mag for the aperture correction from 0".5 to nominal infinity provided by the STScI in this study, whereas Lee & Jang (2012) used an aperture correction of 0.04 mag, which was derived from the data of M101. The latter value of aperture correction based on a small number of bright stars in M101 turned out to be an underestimation. Second is the difference in the images of M101 used for analysis. We used the images corrected for charge transfer efficiency in this study, while Lee & Jang (2012) used the images without this correction, which were the only available images at that time.

The TRGB distances to these galaxies were obtained by applying the TRGB calibrations, the blue I and the QT calibrations, given in Paper IV. A summary of the TRGB distances of these five galaxies is included in **Table 2**. The distance moduli to the eight SN Ia host galaxies from the two TRGB calibrations show good agreement. A weighted mean of distance modulus differences between two calibrations is only $\Delta(m - M)_0 = 0.012 \pm 0.021$ mag, when both NGC 4258 and the LMC are used for the TRGB zero-point. We use the distance estimates from the QT calibration based on two distance anchors, NGC 4258 and the LMC, in the following anal-

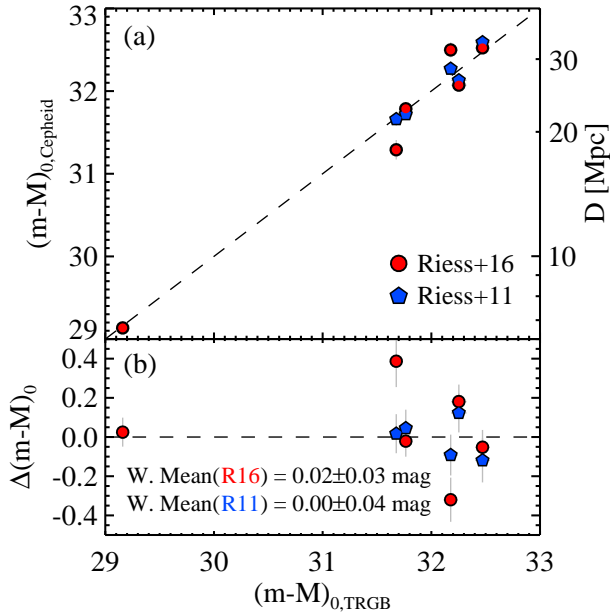


FIG. 8.— (a) Comparison of distance estimates to SN Ia host galaxies derived in this study based on the TRGB with previous studies based on Cepheids: Riess et al. (2016) (circles) and Riess et al. (2011) (pentagons). (b) Differences $\Delta(m - M)_0 = (m - M)_{0,\text{TRGB}} - (m - M)_{0,\text{Cepheids}}$ between this study and the previous studies. Weighted mean values of the difference between two studies are labeled. Note that one outlier with $\Delta(m - M)_0 \approx 0.4$ is NGC 4038/39.

ysis.

4.2. Comparison with the SH0ES Project

The SH0ES project has been working on the calibration of SN Ia to measure an accurate value of the Hubble constant as well as other cosmological parameters (Riess et al. 2005, 2009a,b, 2011, 2016). They used Cepheid variables, a Population I indicator, for deriving distances to SN Ia host galaxies. Riess et al. (2011, 2016) considered four nearby distance anchors for the calibration of Cepheids: NGC 4258, the LMC, the Milky Way, and M31. They provided Cepheid distance estimates to SN Ia host galaxies based on three anchors (NGC 4258, the LMC, and the Milky Way) in Table 3 of Riess et al. (2011) and in Table 5 of Riess et al. (2016). Among 19 and 8 SN Ia host galaxies used in Riess et al. (2016) and Riess et al. (2011), 6 (M101, NGC 4038/39, NGC 5584, NGC 3021, NGC 3370, and NGC 1309) and 5 galaxies (the above excluding M101), respectively, are common with those in this study. Thus, we compare distance estimates of these galaxies derived in this study with those in Riess et al. (2011, 2016), summarizing the results in **Table 3**.

Figure 8(a) displays a comparison of the TRGB distance estimates to SN Ia host galaxies derived in this study with Cepheid distance estimates to 6 galaxies in Riess et al. (2016) (circles) and 5 galaxies in Riess et al. (2011) (pentagons). Differences of distance estimates, $\Delta(m - M)_0 = (m - M)_{0,\text{TRGB}} - (m - M)_{0,\text{Cepheids}}$, are shown in **Figure 8(b)**. Riess et al. (2011) adopted a megamaser distance to NGC 4258 of $(m - M)_0 = 29.31 \pm 0.05$, which is slightly smaller than the value used in Riess et al. (2016) and this study, $(m - M)_0 = 29.387 \pm 0.057$. Riess et al. (2016) slightly improved the estimate

of NGC 4258 distance given by Humphreys et al. (2013) and presented an updated value. However, the distance values in Table 3 of Riess et al. (2011) and Table 5 of Riess et al. (2016) are based on the combination of three anchors (NGC 4258, the LMC, and the MW) so the effect of the change for NGC 4258 alone is not as large as 0.077 mag. Riess et al. (2016) presented a comparison of their results with those in Riess et al. (2011) for the seven common galaxies (except for NGC 4038/39): the mean difference ($\Delta(m - M)_0 = \text{Riess et al. (2016)} - \text{Riess et al. (2011)}$) is 0.01 mag with a dispersion of 0.12 mag. They noted, however, that the distance difference for NGC 4038/39 (antennae galaxies) hosting SN 2007sr is as large as $\Delta(m - M)_0 = -0.37$. This large difference is due to removing 10 Cepheids with ultra-long periods (ULP, $P > 100$ days) in the sample of Cepheids for NGC 4038/39 during the new analysis of Riess et al. (2016).

The TRGB distance estimates in this study and the Cepheid distance estimates in Riess et al. (2011) and Riess et al. (2016) show excellent agreement. One outlier seen at $\Delta(m - M)_0 = 0.387 \pm 0.118$ of **Figure 8(b)** is NGC 4038/39. A weighted mean of distance difference for the five galaxies between this study and Riess et al. (2011) is very small: $\Delta(m - M)_0 = 0.001 \pm 0.039$ mag with a standard deviation of 0.098 mag. A comparison with Riess et al. (2016) for the six overlapping galaxies yields a similar offset, $\Delta(m - M)_0 = 0.022 \pm 0.028$ mag, but its standard deviation is larger than that from Riess et al. (2011). If we exclude NGC 4038/39 in the comparison, the mean difference between this study and Riess et al. (2016) becomes zero, $\Delta(m - M)_0 = -0.000 \pm 0.029$ mag.

In summary, our TRGB distance estimates are in good agreement with the Cepheid distance estimates in Riess et al. (2011, 2016). A better agreement is seen with those in Riess et al. (2016), if we exclude NGC 4038/39.

4.3. A Distance Discrepancy for NGC 4038/39

The significant difference ($\Delta(m - M)_{0,\text{TRGB}} - \text{Cepheid} = 0.387 \pm 0.118$) for NGC 4038/39 between the TRGB distance in this study and the Cepheid distance in Riess et al. (2016) is an interesting issue, deserving an investigation of any cause for this discrepancy. NGC 4038/39 is a pair of interacting galaxies, showing clear features of strong star formation. However, the CMD of the resolved stars derived from deep HST images of a region outside arms in NGC 4038/39 shows a prominent RGB as well as a weaker AGB. Photometry of the RGB stars reaches about 1.5 mag below the TRGB so that the detection of the TRGB is considered to be solid (Jang & Lee 2015). The TRGB distance for NGC 4038/39 in this study and Jang & Lee (2015) is consistent with the previous estimate based on the TRGB by Schweizer et al. (2008), $(m - M)_0 = 31.51 \pm 0.17$. Thus the TRGB distance estimate for this galaxy in this study is considered to be reliable.

On the other hand, two recent studies based on the same data of Cepheids, Riess et al. (2011) and Riess et al. (2016), showed a large discrepancy. The reason for this difference is related with the presence of ULP Cepheids in the Cepheid sample for NGC 4038/39. ULP Cepheids have longer periods ($P > 80$ days) and are brighter ($-6 > M_V > -8$) than classical Cepheids.

TABLE 3
A COMPARISON OF DISTANCE ESTIMATES TO SN IA HOST GALAXIES

Target	This study ^a (TRGB)	R11 ^b (Cepheids)	R16 ^b (Cepheids)	This study – R11	This study – R16
M101	29.160 ± 0.022	...	29.135 ± 0.045	...	0.025 ± 0.050
NGC 4038/39	31.677 ± 0.037	31.66 ± 0.08	31.290 ± 0.112	0.017 ± 0.088	0.387 ± 0.118
NGC 5584	31.751 ± 0.049	31.72 ± 0.07	31.786 ± 0.046	0.031 ± 0.085	−0.035 ± 0.067
NGC 3021	32.178 ± 0.033	32.27 ± 0.08	32.498 ± 0.090	−0.092 ± 0.087	−0.320 ± 0.096
NGC 3370	32.253 ± 0.041	32.13 ± 0.07	32.072 ± 0.049	0.123 ± 0.081	0.181 ± 0.064
NGC 1309	32.471 ± 0.040	32.59 ± 0.09	32.523 ± 0.055	−0.119 ± 0.098	−0.052 ± 0.068
Weighted mean of all				0.001 ± 0.039 ^c	0.022 ± 0.028 ^d
Weighted mean of all excluding NGC 4038/39				−0.003 ± 0.044 ^e	0.000 ± 0.029 ^f

^a Based on two distance anchors: NGC 4258 and the LMC.

^b Based on three distance anchors: NGC 4258, the LMC, and the Milky Way. R11 and R16 denote Riess et al. (2011) and Riess et al. (2016), respectively.

^c Standard deviation of 0.098 mag.

^d Standard deviation of 0.235 mag.

^e Standard deviation of 0.112 mag.

^f Standard deviation of 0.187 mag.

TABLE 4
A SUMMARY OF OPTICAL LUMINOSITY CALIBRATION OF SNE IA

Galaxy	SN Ia	Filters	A_V	$m_V^0 + 5a_V$ This study	$m_V^0 + 5a_V$ Literature	$m_B^0 + 5a_B$ From R16	$(m - M)_0$ TRGB	M_V^0 R11 calibration	M_B^0 R16 calibration
M101	SN 2011fe	UBVRI	0.157	13.400	...	13.310	29.160 ± 0.022	−19.255 ± 0.143	−19.414 ± 0.120
M66	SN 1989B	UBVRI	1.242	14.076	14.021 ^a	...	30.180 ± 0.038	−19.589 ± 0.191	...
M96	SN 1998bu	UBVRI	1.025	14.278	14.263 ^a	...	30.223 ± 0.054	−19.430 ± 0.182	...
N4038/39	SN 2007sr	uBVri	0.349	15.889	15.901 ^b	15.795	31.677 ± 0.037	−19.273 ± 0.149	−19.445 ± 0.125
N5584	SN 2007af	uBVri	0.346	16.295	16.274 ^b	16.264	31.751 ± 0.049	−18.941 ± 0.152	−19.050 ± 0.130
N3021	SN 1995al	BVRI	0.213	16.630	16.699 ^b	16.526	32.178 ± 0.033	−19.033 ± 0.145	−19.215 ± 0.123
N3370	SN 1994ae	UBVRI	0.045	16.556	16.545 ^b	16.474	32.253 ± 0.041	−19.182 ± 0.146	−19.342 ± 0.122
N1309	SN 2002fk	BVRI	0.072	16.774	16.768 ^b	16.755	32.471 ± 0.040	−19.182 ± 0.146	−19.279 ± 0.123
Weighted mean of eight SNe								−19.209 ± 0.055	...
Weighted mean of six low-reddened SNe								−19.147 ± 0.060	−19.295 ± 0.051

^a Note. A_V denotes V -band host galaxy extinction derived from the light curve fitting with the MLCS2k2 code. m_V^0 and m_B^0 indicate the corrected apparent peak magnitude of SN Ia in V and B -band, respectively. a_V ($= 0.697 \pm 0.002$) and a_B ($= 0.7127 \pm 0.0017$) denote the V and B -band intercepts of the SN Ia Hubble diagram.

^a Derived from Jha et al. (2007).

^b Derived from Riess et al. (2011).

They are often found in star-forming late-type galaxies with low-metallicity and their period-luminosity relation is not as well-known as classical Cepheids (Bird et al. 2009; Fiorentino et al. 2012, 2013).

Riess et al. (2016) excluded 10 ULP Cepheids from the sample of Cepheids for NGC 4038/39 used in Riess et al. (2011) for distance estimation, because the phase coverage of these Cepheids is very sparse and because the period-luminosity relation of ULP Cepheids is not as reliable as that of normal Cepheids. From the Cepheid sample without ULP Cepheids, Riess et al. (2016) obtained a distance modulus for NGC 4038/39, 0.37 mag smaller than the value derived from the full sample of Cepheids that was used in Riess et al. (2011). Fiorentino et al. (2013) applied a theoretical scenario for classical Cepheids to the same sample of Cepheids (including ULP Cepheids) in the galaxies as used in Riess et al. (2011). They derived a distance to NGC 4038/39 from the full sample of Cepheids, $(m - M)_0 = 31.55 \pm 0.06$, which is consistent with the value in Riess et al. (2011), but about 0.3 larger than the value given by Riess et al. (2016). NGC 4038/39 shows the largest fraction of ULP Cepheids in the sample of SN

Ia host galaxies used by Riess et al. (2011, 2016), which must be strongly related with active star formation activity. Considering that most of the Cepheids in Cepheid distance anchors are classical Cepheids, it appears to be conservative to use only classical Cepheids in the case of NGC 4038/39. However, it is difficult to understand the large difference between this value and the TRGB distance. A further study is needed to investigate the effect of the ULP Cepheids in Cepheid distance estimation (Fiorentino et al. 2012).

4.4. The Calibration of SNe Ia and the Hubble Constant

With the TRGB distances to SN Ia host galaxies derived in this study, we calibrate the absolute peak luminosity of SNe Ia and estimate the value of the Hubble constant. Optical light curves of eight SNe Ia were obtained from various literature: $UBVRI$ photometric data for SN 2011fe from Pereira et al. (2013), for SN 1989B from Wells et al. (1994), for SN 1998bu from Jha et al. (1999), for SN 1995al from Riess et al. (2009a), $BVRI$ photometric data for SN 1994ae and SN 2002fk from Riess et al. (2009a), and $uBVri$ photometric data

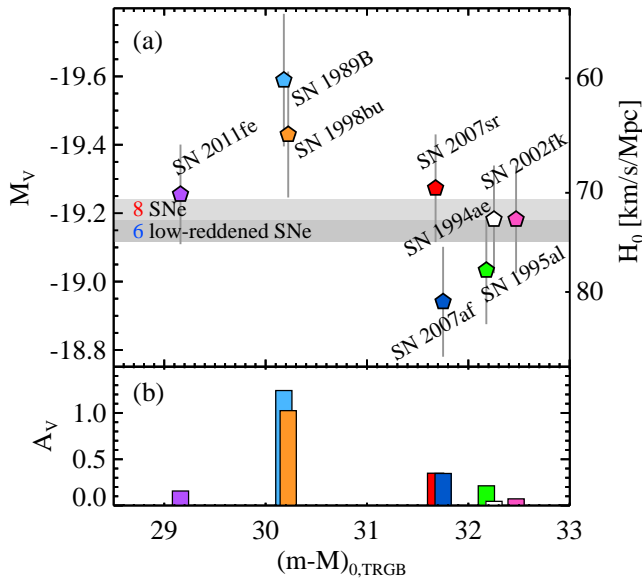


FIG. 9.— (a) Comparison of absolute peak magnitudes of eight SNe Ia with their TRGB distances derived in this study. Two shaded regions indicate weighted means of eight SNe Ia (upper region) and six low-reddened SNe Ia (lower region). (b) Comparison of V -band host galaxy extinction values (A_V) with the TRGB distances. Note that two SNe, SN 1989B in M66 and SN 1998bu in M96, show significantly higher extinctions than those of other six SNe.

for SN 2007sr and SN 2007af from the Carnegie Supernova Program (Hamuy et al. 2006) (u) and Hicken et al. (2009) (BVri). We also compiled three V -band observations at the pre-maximum of SN 2007sr provided by the All-Sky Automated Survey (ASAS) (Pojmanski 1997) and Riess et al. (2011). All eight SNe Ia were observed with CCD detectors, so that detector dependent uncertainties are estimated to be smaller than those from photographic or photoelectric detectors.

We derived light-curve parameters of each SN Ia using the MLCS2K2 code (version 0.07) (Jha et al. 2007). We set total to selective extinction ratio, $R_V = 3.1$ for the Milky Way and $R_V = 2.5$ for the SN Ia host galaxies, to be consistent with the values used in Riess et al. (2011, 2016). The derived values of the parameters, A_V and $m_V^0 + 5a_V$ (where $a_V = 0.697 \pm 0.002$ (Riess et al. 2011)), are listed in Table 4. We also listed the $m_V^0 + 5a_V$ values from Jha et al. (2007) and Riess et al. (2011) in column six of Table 4. The values of $m_V^0 + 5a_V$ derived in this study agree well with those from Jha et al. (2007) and Riess et al. (2011), showing a mean difference of 0.004 mag. Absolute maximum magnitudes of eight SNe Ia, corrected to the fiducial color and luminosity, were also derived from the m_V^0 values and the TRGB distances derived in this study, as listed in the column nine of Table 4. Quoted uncertainties are quadratic sums of the TRGB distance errors, extinction errors (10% of the Milky Way and the host galaxy extinction values), and the luminosity dispersion of SNe Ia, 0.14 mag (Jha et al. 2007).

Figure 9 displays distributions of V -band absolute maximum magnitudes (M_V^0) and host galaxy extinction values (A_V) of SNe Ia as a function of the TRGB distances derived in this study. Absolute magnitudes of SNe Ia range from $M_V^0 = -18.941$ (SN 2007af) to

-19.589 (SN 1989B). Host galaxy extinction values are estimated to be small, except for two SNe. SN 1989B and SN 1998bu show significantly higher extinction values ($A_V > 1.0$) than those of other SNe ($A_V < 0.4$). Thus derived absolute magnitudes for these two highly reddened SNe are probably less reliable than the others, although we corrected for their extinctions. The standard deviation of all eight SNe and six low-reddened SNe are 0.206 mag and 0.131 mag, respectively. The former is slightly larger than the intrinsic luminosity dispersion of SNe Ia derived from a large sample of SNe, 0.14 mag (Jha et al. 2007) and 0.128 mag (Riess et al. 2016). On the other hand, the value for the six low-reddened SNe is similar to the intrinsic luminosity dispersion of SNe.

A weighted mean of the absolute peak magnitude of eight SNe is $M_V^0 = -19.209 \pm 0.055$ mag. It is 0.089 mag brighter than that from the SHOES project (Riess et al. 2011, 2016) ($M_V^0 = -19.12$ mag). If we use six low-reddened SNe, then a weighted mean of the absolute peak magnitude would be slightly fainter, $M_V^0 = -19.147 \pm 0.060$, getting closer to the estimate by Riess et al. (2011, 2016). Riess et al. (2016) provided SALT-II fits of 19 SNe Ia including the 6 low-reddened SNe used in this study. They did not include 2 highly reddened SNe, SN 1989B and SN 1998bu. The values of $m_B^0 + 5a_B$ provided by Riess et al. (2016) are listed in column 7 of Table 4. The B -band absolute magnitudes of SNe Ia (M_B^0) were derived from the m_B^0 values in Riess et al. (2016) and the TRGB distance estimates in this study, as listed in the last column of Table 4. A weighted mean of the B -band absolute magnitudes of the six SNe is $M_B^0 = -19.295 \pm 0.051$ mag. It is 0.045 mag brighter than that given in Riess et al. (2016), $M_B^0 = -19.25$ mag.

Riess et al. (2011, 2016) used an equation deriving the value of H_0 from the absolute magnitude of SNe Ia:

$$\log H_0 = \frac{M_x^0 + 5a_x + 25}{5}$$

where M_x^0 is an absolute magnitude of SNe Ia and a_x is an intercept of the SN Ia Hubble diagram in band- x .

Riess et al. (2011) presented a value of $a_V (= 0.697 \pm 0.00201)$ that was determined from the MLCS2k2 fits of 140 SNe Ia at $0.023 < z < 0.10$. Combining the above equation with the V -band absolute magnitudes of SN Ia derived in this study, we derive a value of the Hubble constant: $H_0 = 71.66 \pm 1.80(\text{random}) \pm 1.88(\text{systematic})$ km s $^{-1}$ Mpc $^{-1}$ from the eight SNe, and $H_0 = 73.72 \pm 2.03(\text{random}) \pm 1.94(\text{systematic})$ km s $^{-1}$ Mpc $^{-1}$ from the six low-reddened SNe.

Riess et al. (2016) provided an updated value, $a_B = 0.7127 \pm 0.0017$ from the SALT-II fits of 233 SNe at $0.023 < z < 0.15$. If we use this value and the sample of six low-reddened SNe, we obtain our best estimate of the Hubble constant, which is accurate to 3.51% (± 2.50 km s $^{-1}$ Mpc $^{-1}$) including the systematics: $H_0 = 71.17 \pm 1.66(\text{random}) \pm 1.87(\text{systematic})$ km s $^{-1}$ Mpc $^{-1}$. Riess et al. (2016) also present a value of the Hubble constant, when only two distance anchors (NGC 4258 and the LMC) are used for Cepheid distances: $H_0 = 71.61 \pm 1.78$ km s $^{-1}$ Mpc $^{-1}$. Thus, our best estimate is consistent with this value. This shows that the TRGB and the Cepheid produce distance results consistent with each other, as long as the same distance

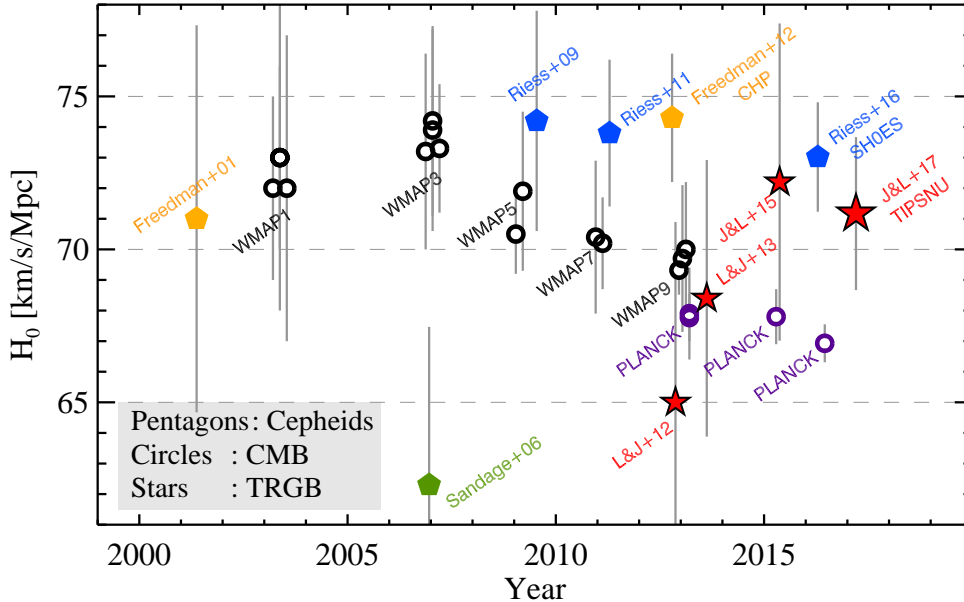


FIG. 10.— Comparison of recent values of the Hubble Constant based on the TRGB calibration of SN Ia (starlets), the Cepheid calibration of SN Ia (pentagons), and the WMAP and Planck CMBR results (circles). Note that our best TRGB estimate in this study is between the 2016 Cepheid value and recent Planck values.

anchors are used.

In **Figure 10**, we compare recent values of the Hubble constant based on the TRGB calibration of SN Ia in this study, including Lee & Jang (2012, 2013), Jang & Lee (2015) the Cepheid calibration of SN Ia (Freedman et al. 2001; Sandage et al. 2006; Riess et al. 2009b, 2011; Freedman et al. 2012; Riess et al. 2016), and the WMAP and PLANCK CMBR results. Our best estimate is between the values from the Cepheid calibrated SNe Ia based on all four distance anchors and those from the CMB analysis. The levels of differences between our best estimate and the values from other studies are: 1.70σ with Planck Collaboration et al. (2015) (PLANCK), 0.92σ with Bennett et al. (2013) (WMAP9), 0.56σ with Riess et al. (2016) (SH0ES), 0.88σ with Riess et al. (2011) (SH0ES), and 1.08σ with Freedman et al. (2012) (CHP-I). Thus, our estimate agrees, within 1.7σ , with the recent estimations based on Cepheid calibrated SNe Ia and the CMB analysis. The Cepheid calibrated results in Riess et al. (2016) heighten the Hubble tension. On the other hand, our TRGB calibrated results are comfortably located between the Cepheid results and the CMB results, lowering the Hubble tension.

In this study, we used two distance anchors, NGC 4258 and the LMC, while recent Cepheid studies (Riess et al. 2011, 2016) utilized two more anchors, the Milky Way Cepheids with parallaxes and M31 for which geometric distances of two DEBs are known (Ribas et al. 2005; Vilardell et al. 2010) ($(m - M)_0 = 24.36 \pm 0.08$). Note that the two anchors used in this study lead to a slightly lower value of the Hubble Constant based on Cepheids, than the other two anchors, the Milky Way and M31: $H_0 = 72.2 \pm 2.51$ for NGC 4258, $H_0 = 72.04 \pm 2.67$ for the LMC, $H_0 = 76.18 \pm 2.37$ for the Milky Way, and $H_0 = 74.50 \pm 3.27$ for M31 $\text{km s}^{-1} \text{Mpc}^{-1}$ (Riess et al. 2016). Thus it is important to understand any causes for this difference and to reduce this difference in the future.

We are planning to investigate M31 as another anchor for the TRGB in the near future. When GAIA astrometry of the Milky Way stars is available, a number of TRGB stars in the Milky Way can be used for absolute calibration of the TRGB magnitudes so they can serve as a distance anchor for the TRGB (de Bruijne et al. 2014; Beaton et al. 2016).

5. SUMMARY

Using deep photometry of the resolved stars in the HST images, we determine TRGB distances to three SN Ia host galaxies: NGC 3021 hosting SN 1995al, NGC 3370 hosting SN 1994ae, and NGC 1309 hosting SN 2002fk. We combine these results with those in our previous studies and calibrate the luminosity of SN Ia. Then we estimate the value of the Hubble Constant using the SN Ia with the TRGB calibration. Primary results are as follows.

- We find a significant number of old RGB stars in the halo regions of the three galaxies, presenting their CMDs.
- Applying the revised TRGB calibration introduced by Jang & Lee (2017) (Paper IV) we measured the TRGB magnitudes, obtaining $QT_{\text{RGB}} = 28.146 \pm 0.033$ for NGC 3021, 28.212 ± 0.041 for NGC 3370 and 28.398 ± 0.040 for NGC 1309. From these, we derive TRGB distances: $(m - M)_0 = 32.178 \pm 0.033$ for NGC 3021, 32.253 ± 0.041 for NGC 3370, and 32.471 ± 0.040 for NGC 1309.
- We updated our previous distance estimates to five SN Ia host galaxies (M101, M66, M96, NGC 4038/39 and NGC 5584), as listed in **Table 2**, applying the revised TRGB calibration.
- We compared our TRGB distance estimates with the Cepheid distance estimates presented in

Riess et al. (2011) and Riess et al. (2016), obtaining

$\Delta(m - M)_0(\text{TRGB} - \text{Cepheid}) = 0.001 \pm 0.039$ mag for five common galaxies in Riess et al. (2011), 0.022 ± 0.028 mag for six common galaxies in Riess et al. (2016), and 0.000 ± 0.029 mag for five galaxies (excluding NGC 4038/39) in Riess et al. (2016).

- Our TRGB distance to NGC 4038/39 is significantly larger than the Cepheid distance given by Riess et al. (2016) ($\Delta(m - M)_0(\text{TRGB} - \text{Cepheid}) = 0.387 \pm 0.118$), while it is similar to the Cepheid distance given by Riess et al. (2011). The difference in the Cepheid distance between Riess et al. (2011) and Riess et al. (2016) is due to the presence of ULP Cepheids in this galaxy. This shows that the Cepheid distance estimation of active star-forming galaxies can be affected significantly by the ULP Cepheids.

- From the mean absolute peak magnitude of the six low-reddened SNe Ia and the recent SN Ia calibration in Riess et al. (2016), we derive our best estimate of the Hubble constant: $H_0 = 71.17 \pm 1.66(\text{random}) \pm 1.87(\text{systematic}) \text{ km s}^{-1} \text{ Mpc}^{-1}$. This estimate is between the values from the Cepheid calibrated SNe Ia (Riess et al. 2011; Freedman et al. 2012; Riess et al. 2016) and those from the CMB analysis (Bennett et al. 2013; Planck Collaboration et al. 2015). This alleviates the Hubble tension between the Cepheid results and CMB results.

The authors are grateful to the anonymous referee for his/her comments that improved the original manuscript and to Adam Riess for useful discussions on Cepheid distances to SN Ia host galaxies. This work was supported by the National Research Foundation of Korea (NRF) grant funded by the Korea Government (MSIP) (No. 2012R1A4A1028713). This paper is based on image data obtained from the Multimission Archive at the Space Telescope Science Institute (MAST).

REFERENCES

- Aubourg, É., Bailey, S., Bautista, J. E., et al. 2015, *Phys. Rev. D*, 92, 123516
- Beaton, R. L., Freedman, W. L., Madore, B. F., et al. 2016, *ApJ*, 832, 210
- Bennett, C. L., Larson, D., Weiland, J. L., et al. 2013, *ApJS*, 208, 20
- Bird, J. C., Stanek, K. Z., & Prieto, J. L. 2009, *ApJ*, 695, 874
- de Bruijne, J. H. J., Rygl, K. L. J., & Antoja, T. 2014, *EAS Publications Series*, 67, 23 *Gaia Astrometric Science Performance - Post-Launch Predictions*
- de Vaucouleurs, G., & Peters, W. L. 1981, *ApJ*, 248, 395
- de Vaucouleurs, G. 1993, *ApJ*, 415, 10
- Fiorentino, G., Clementini, G., Marconi, M., et al. 2012, *Ap&SS*, 341, 143
- Fiorentino, G., Musella, I., & Marconi, M. 2013, *MNRAS*, 434, 2866
- Fiorentino, G., Annibali, F., Clementini, G., et al. 2013, *Advancing the Physics of Cosmic Distances*, 289, 282
- Freedman, W. L., Madore, B. F., Gibson, B. K., et al. 2001, *ApJ*, 553, 47
- Freedman, W. L., & Madore, B. F. 2010, *ARA&A*, 48, 673
- Freedman, W. L., Madore, B. F., Scowcroft, V., et al. 2012, *ApJ*, 758, 24
- Hamuy, M., Folatelli, G., Morrell, N. I., et al. 2006, *PASP*, 118, 2
- Hicken, M., Challis, P., Jha, S., et al. 2009, *ApJ*, 700, 331
- Humphreys, E. M. L., Reid, M. J., Moran, J. M., Greenhill, L. J., & Argon, A. L. 2013, *ApJ*, 775, 13
- Illingworth, G. D., Magee, D., Oesch, P. A., et al. 2013, *ApJS*, 209, 6
- Jang, I. S., & Lee, M. G. 2015, *ApJ*, 807, 133 (Paper III)
- Jang, I. S., & Lee, M. G. 2017, *ApJ*, in press (arXiv:1611.05040) (Paper IV)
- Jha, S., Garnavich, P. M., Kirshner, R. P., et al. 1999, *ApJS*, 125, 73
- Jha, S., Riess, A. G., & Kirshner, R. P. 2007, *ApJ*, 659, 122
- Lee, M. G., Freedman, W. L., & Madore, B. F. 1993, *ApJ*, 417, 553
- Lee, M. G., & Jang, I. S. 2012, *ApJ*, 760, L14 (Paper I)
- Lee, M. G., & Jang, I. S. 2013, *ApJ*, 773, 13 (Paper II)
- Lee, M. G., & Jang, I. S. 2016, *ApJ*, 831, 108
- Madore, B. F., & Freedman, W. L. 1995, *AJ*, 109, 1645
- Pereira, R., Thomas, R. C., Aldering, G., et al. 2013, *A&A*, 554, AA27
- Pietrzyński, G., Graczyk, D., Gieren, W., et al. 2013, *Nature*, 495, 76
- Planck Collaboration, Ade, P. A. R., Aghanim, N., et al. 2015, arXiv:1502.01589
- Pojmanski, G. 1997, *Acta Astronomica*, 47, 467 *The All Sky Automated Survey*
- Ribas, I., Jordi, C., Vilardell, F., et al. 2005, *ApJ*, 635, L37
- Riess, A. G., Li, W., Stetson, P. B., et al. 2005, *ApJ*, 627, 579
- Riess, A. G., Macri, L., Li, W., et al. 2009, *ApJS*, 183, 109
- Riess, A. G., Macri, L., Casertano, S., et al. 2009, *ApJ*, 699, 539
- Riess, A. G., Macri, L., Casertano, S., et al. 2011, *ApJ*, 730, 119
- Riess, A. G., Macri, L. M., Hoffmann, S. L., et al. 2016, *ApJ*, 826, 56
- Rizzi, L., Tully, R. B., Makarov, D., et al. 2007, *ApJ*, 661, 815
- Sandage, A., & Tammann, G. A. 1974, *ApJ*, 190, 525
- Sandage, A., & Tammann, G. A. 1974, *ApJ*, 191, 603
- Sandage, A., & Tammann, G. A. 1974, *ApJ*, 194, 223
- Sandage, A., & Tammann, G. A. 1974, *ApJ*, 194, 559
- Sandage, A., & Tammann, G. A. 1975, *ApJ*, 196, 313
- Sandage, A., & Tammann, G. A. 1975, *ApJ*, 197, 265
- Sandage, A., & Tammann, G. A. 1976, *ApJ*, 210, 7
- Sandage, A., Tammann, G. A., Saha, A., et al. 2006, *ApJ*, 653, 843
- Schlafly, E. F., & Finkbeiner, D. P. 2011, *ApJ*, 737, 103
- Schweizer, F., Burns, C. R., Madore, B. F., et al. 2008, *AJ*, 136, 1482
- Stetson, P. B. 1987, *PASP*, 99, 191
- Stetson, P. B. 1994, *PASP*, 106, 250
- van den Bergh, S. 1960, *ZAp*, 49, 198
- van den Bergh, S. 1960, *JRASC*, 54, 49
- van den Bergh, S. 1975, *Galaxies and the Universe*, 509 *Galaxies and the Universe* (Edited by Allan Sandage, Mary Sandage, and Jerome Kristian), University of Chicago Press (Stars and Stellar Systems. Volume 9), Chicago.
- van den Bergh, S. 1994, *PASP*, 106, 1113
- Vilardell, F., Ribas, I., Jordi, C., Fitzpatrick, E. L., & Guinan, E. F. 2010, *A&A*, 509, A70
- Wells, L. A., Phillips, M. M., Suntzeff, B., et al. 1994, *AJ*, 108, 2233